Energies **2014**, *7*, 4588-4600; doi:10.3390/en7074588

OPEN ACCESS

energies

ISSN 1996-1073

www.mdpi.com/journal/energies

Discussion

Understanding of Sulfurized Polyacrylonitrile for Superior Performance Lithium/Sulfur Battery

Sheng S. Zhang

Electrochemistry Branch, RDRL-SED-C, Sensors and Electron Devices Directorate,
U.S. Army Research Laboratory, Adelphi, MD 20783-1197, USA;
E-Mail: shengshui.zhang.civ@mail.mil or shengshui@gmail.com;
Tel.: +1-301-394-0981; Fax: +1-301-394-0273

Received: 20 May 2014; in revised form: 17 June 2014 / Accepted: 10 July 2014 / Published: 18 July 2014

Abstract: Sulfurized polyacrylonitrile (SPAN) is one of the most important sulfurized carbon materials that can potentially be coupled with the carbonaceous anode to fabricate a safe and low cost "all carbon" lithium-ion battery. However, its chemical structure and electrochemical properties have been poorly understood. In this discussion, we analyze the previously published data in combination with our own results to propose a more reasonable chemical structure that consists of short $–S_x–$ chains covalently bonded onto cyclized, partially dehydrogenated, and ribbon-like polyacrylonitrile backbones. The proposed structure fits all previous structural characterizations and explains many unique electrochemical phenomena that were observed from the Li/SPAN cells but have not been understood clearly.

Keywords: lithium-sulfur battery; sulfur cathode; sulfurized carbon; sulfurized polyacrylonitrile; polysulfide

1. Introduction

Sulfurized carbons are a class of new cathode materials, which have recently attracted considerable interest in developing high energy density rechargeable lithium/sulfur (Li/S) batteries [1]. Among numerous potential candidates, sulfurized polyacrylonitrile (SPAN) has been most intensively studied due to its excellent electrochemical performance and low process cost. The synthesis of SPAN was first reported in 2002 by Wang *et al.* who heated a 5:1 (wt) S/PAN mixture at 280–300 °C under argon for 6 h [2,3], and since intensive investigations have been followed, especially by the groups

led by He [4–8], Buchmeiser [9–11], and Chen [12–15]. Most of previous works were focused on the structural characterization, the optimization of synthesis conditions in variations of reaction temperature, reaction time and S/PAN ratio, as well as the applications with different electrolyte systems [4–20].

During heating, PAN polymer chains are cyclized and dehydrogenated by losing small hydrogen sulfide (H_2S) molecules, the resulting carbon double bonds are instantly sulfurized (vulcanized) by small sulfur fragments. Therefore, the original PAN structure no longer remains in the final product, the term of SPAN cannot reflect the true chemical structure so that alternative terms such as conducting polymer and composite have also been used to describe this type of materials. The reported advantages of the SPAN over elemental sulfur include: (1) it offers very stable specific capacity close to or even higher than the theoretical value of elemental sulfur; (2) it completely avoids the dissolution of long-chain lithium polysulfide (PS) in organic electrolyte, as well as the resulting redox shuttle and parasitic reactions with lithium anode; (3) it is chemically compatible with the $LiPF_6$-carbonate based electrolytes widely used in the state-of-art Li-ion batteries; (4) it suits for the cathode with high active material loading; and (5) the Li/SPAN cell after activation has nearly 100% coulombic efficiency (CE) and extremely low self-discharge rate. Moreover, He *et al.* have successfully demonstrated a proof-of-concept "all carbon" Li-ion battery by electrochemically pre-lithiating a graphite anode and then coupling the pre-lithiated graphite anode with a SPAN cathode [6]. The dream to fabricate safe and low cost metal-free Li-ion batteries will become true once a viable process for the pre-lithiation of either SPAN cathode or carbonaceous (or others such as silicon, tin, and their relative alloys) anode can be successfully developed.

Despite the superior performances stated above, the chemical structure and electrochemical properties of the SPAN materials have never been understood clearly. The state of sulfur in the SPAN materials is still in debate. Some authors considered the elemental sulfur is embedded in the pyrolyzed PAN backbones in the form of nano-sized sulfur particles [2,12]. Other authors believed the sulfur is covalently bonded onto the pyrolyzed PAN backbones in the form of short $–S_x–$ chains [9,16]. In addition, many unusual phenomena, such as the significant voltage hysteresis and unusually high irreversible capacity in the first discharge, have been repeatedly reported but have never been understood clearly. It is essential to identify the chemical structure and clearly understand these unique electrochemical properties of the Li/SPAN batteries for further development of this promising cathode material. The purpose of this discussion is to determine a more reasonable chemical structure for the SPAN materials by analyzing the previously published data, and to understand the unique electrochemical phenomena of the Li/SPAN cells.

2. Results and Discussion

2.1. Chemical Structure of Sulfurized Polyacrylonitrile (SPAN)

Many spectroscopic characterizations have consistently identified that sulfurs in the SPAN are present in the form of short $–S_x–$ chains covalently bonded to the cyclized and dehydrogenated PAN backbones through C–S bonds [8–10,16,17]. The group peaks at 1600–1200 cm^{-1} and characteristic peak at 802 cm^{-1} in the Fourier Transform Infrared Spectroscopy (FTIR) spectra are good indications of the dehydrogenated six-membered ring structure containing unsaturated carbon double bonds and heteroatoms [16]. The most direct evidence for the S–S and C–S covalent bonds are the strong signals

of C_2S^-, CNS^-, C_3NS^-, and S_3^- fragments (at m/z = 56, 58, 82, 96, respectively) in the Time-of-Flight Secondary Ion Mass Spectrometry (ToF-SIMS) [9]. Raman spectra give more evidence for the S–S and C–C bonds, as shown in Figure 1. It is indicated that in addition to three common peaks for the S–S stretching, the SPANs display three additional peaks at 305, 374, and 927 cm^{-1} in comparison with elemental sulfur. These three additional peaks can be reasonably assigned to the C–S bonds [16]. In addition, the SPANs exhibit two intense absorption bands at around 1325 and 1513 cm^{-1}, which are respectively attributed to the stretching of G mode sp^2 carbon-bonds in the graphite plane, and the breathing of D mode sp^3 carbon-bonds in the disordered carbon [21]. The intensity of these peaks/bands varies with the reaction temperature and reaction time. In general, the signal intensity ratios of the S–C to S–S and of G mode to D mode are increased with the reaction temperature and the reaction time, reflecting the fact that the length of $–S_x–$ chains decreases and the degree of graphitization increases with the reaction temperature and reaction time. The covalent bonding of sulfur to the polymer backbones has been also indirectly verified by two experiments of (1) the solvent (toluene) extraction showing that the sulfur in the SPAN is unextractable [9] and (2) the thermogravimetric analysis (TGA) showing that the sulfur in the SPAN cannot be completely removed even at above 800 °C [10,12]. Based on the results above, two structures as shown by Structure–a and Structure–b in Scheme 1 were proposed by Yu *et al.* [16] and Fanous *et al.* [9], respectively. In both structures, the short $–S_x–$ chains are covalently bonded to the cyclized and dehydrogenated PAN backbones through the C–S bonds. However, these two structures do not match the results of elemental analyses, which were reported by four independent research groups and are summarized in Table 1. The results of elemental analyses consistently reveal that the SPANs contain 0.89%–1.3% H, which corresponds to a 2.8–2.9 C/H ratio, no matter how long the reaction time is. This means that every three carbons contain at least one hydrogen, which is missed in Structure–a and Structure–b. The significant amounts of hydrogen in the SPANs are also verified by the thermogravimetric analysis-mass spectrometry (TG-MS) analysis, which shows that large amount of H_2S is released in the temperature range of 300–400 °C [10]. Although a > NH functional group is proposed in Structure–b, the IR very sensitive N–H absorptions do not show up in the FTIR spectra [8,12,16,17].

Figure 1. Raman spectra for (a) sulfur, and sulfurized polyacrylonitrile (SPAN) made by heating a 4:1 (wt) S/PAN mixture for 8 h at temperature of (b) 250 °C; (c) 300 °C; (d) 450 °C; and (e) 800 °C. Reproduced with permission of Elsevier from [16].

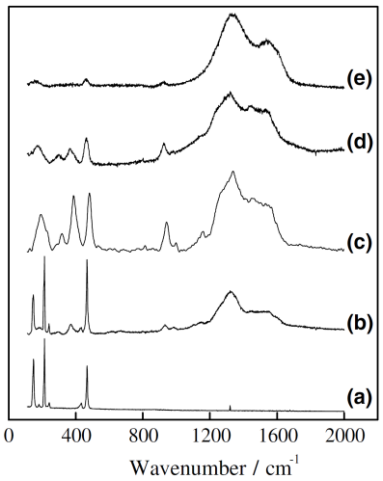

Based on the results of the elemental analyses and TG-MS analysis, we consider that the SPANs are more likely in the structure as indicated by Structure–c in Scheme 1, which is present in the form of two resonance structures. In addition, Table 1 shows that all SPANs have a C/N ratio of slightly greater than 3, implying that the mild denitrogenation must occur in the synthesis of SPANs. Therefore, Structure–c can be further modified as Structure–d, in which the short $–S_x–$ chains are covalently bonded to the cyclized, partially dehydrogenated, and ribbon-like PAN backbones. Structure–d has a C/H ratio equal to 3.0, still slightly greater than the measured values (2.8–2.9), namely, the determined hydrogens are more than expected for Structure–d. The extra hydrogens are due to the incomplete dehydrogenation of the PAN, which is greatly affected by the reaction temperature and reaction time.

Scheme 1. Proposed chemical structures for SPAN. (**a**) Structure–a; (**b**) Structure–b; (**c**) Structure–c; (**d**) Structure–d.

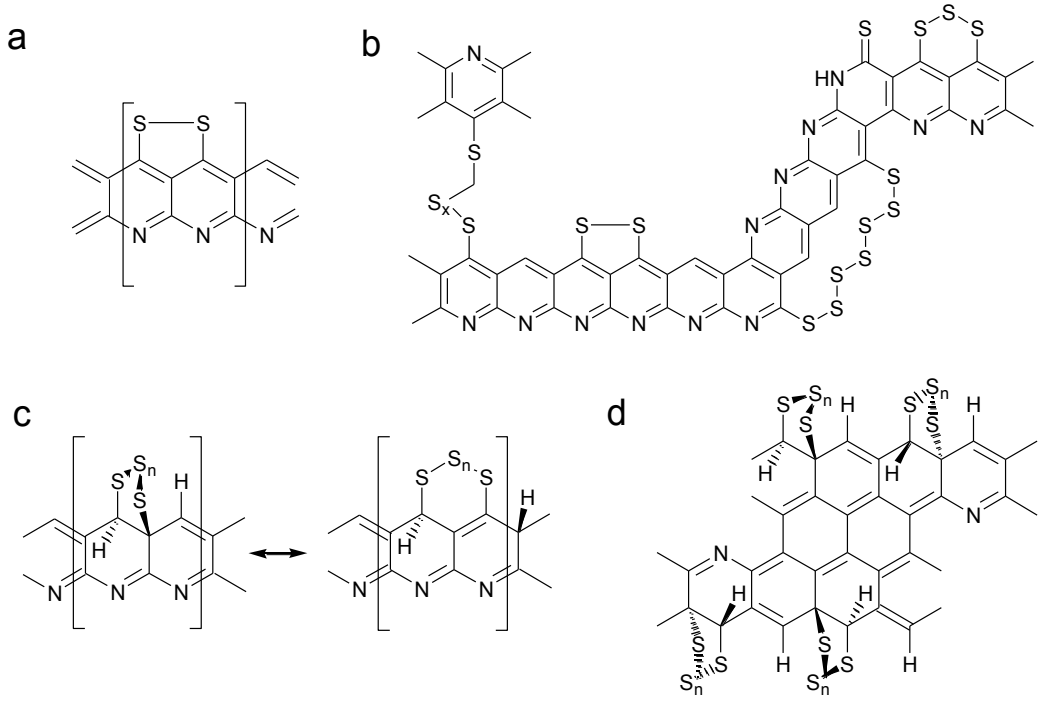

Table 1. Summary of elemental analysis results on sulfurized polyacrylonitriles (SPANs) made by different conditions.

Synthesis Condition	Result, %				Ratio of Element			Source
	S	N	C	H	C/N	C/S	C/H	
280–300 °C, 6 h	53.41	10.73	30.92	0.89	3.36	1.55	2.92	[2]
330 °C, 6 h	41 ± 1	18.2	53	1.7	3.4	–	2.62	[9]
280–300 °C, time 1	46.3	14.4	38.1	1.1	3.09	2.20	2.91	[7]
time 2 (>time 1)	42	15.6	41.2	1.2	3.08	2.62	2.89	–
time 3 (>time 2)	33.7	16.5	43.6	1.3	3.08	3.45	2.82	–
300 °C, 8 h	43.28	13.99	38.12	–	3.17	2.34	–	[16]
450 °C	35.24	15.17	40.80	–	3.13	3.08	–	–
800 °C	15.32	19.05	52.28	–	3.20	8.98	–	–

The averaged length (x value) of $–S_x–$ chains in Structure–c and Structure–d can be roughly estimated by TGA, based on the fact that the C–S bond has much higher standard bond energy than the S–S bond, *i.e.*, 740 kJ mol^{-1} for the C–S bond and 418 kJ mol^{-1} for the S–S bond at 298 K [22]. Figure 2 displays the TGA traces of elemental sulfur and a SPAN containing 49.1% S. In comparison with elemental sulfur that starts subliming at ~200 °C and entirely disappears at around 300 °C, the weight loss of SPAN can be distinctly divided into two regions according to the rate of weight loss, *i.e.*, the fast weight loss region between 220 and 410 °C, and the slow weight loss region above 410 °C. The fast weight loss region is assigned to the breakdown of S–S bonds, and the slow weight loss region to that of S–C bonds. This assignment agrees with the TG-MS results, which show that the thermal decomposition products below 400 °C are dominated by H_2S and those above 400 °C by CS_2 [10]. From the weight loss below 410 °C and the total sulfur content determined by the elemental analysis in the SPAN, it is estimated that ~20% S are present in the form of the S–S bonds and 29.1% S (=49.1%–20%) are in the form of C–S bonds, which lead to an averaged n value of 1.37 in Structure–c. In other words, the averaged x value in the $–S_x–$ chains for the SPAN containing 49.1% S is 3.37 (*i.e.*, $x = n + 2$ in Structure–c and Structure–d of Scheme 1). Thus, the chemical structure of the SPAN can be generally described as the short $–S_x–$ chains covalently bonded to the cyclized, partially dehydrogenated, and ribbon-like PAN backbones. Judged from the results of Figure 2 and Reference 12, it is believed that the maximum x value in SPANs is not greater than 4, otherwise, in discharge the $–S_x–$ chains would disproportionation into even longer polysulfide, leading to polysulfide redox shuttle and poor cyclability.

Figure 2. thermogravimetric analysis (TGA) traces of elemental sulfur and SPAN (49.1% S), made by heating a 4:1 (wt) S/PAN mixture at 300 °C for 4 h. Plotted from the data of [12].

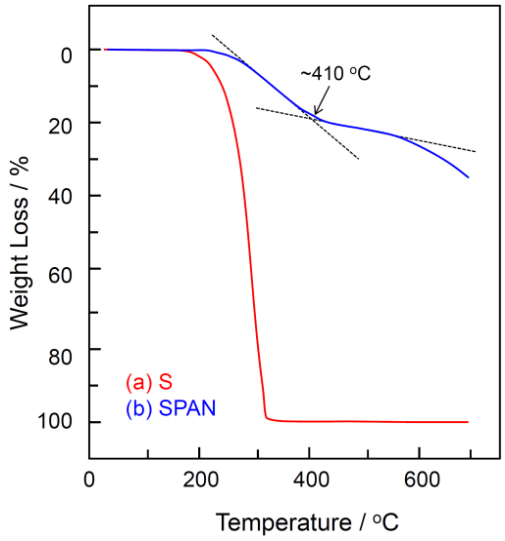

2.2. Electrochemical Characteristics of Li/SPAN Cell

2.2.1. Electrochemical Mechanism

According to Structure–c, the overall reaction of the Li/SPAN cell can be described as Scheme 2:

Scheme 2. Overall reaction of Li/SPAN cell.

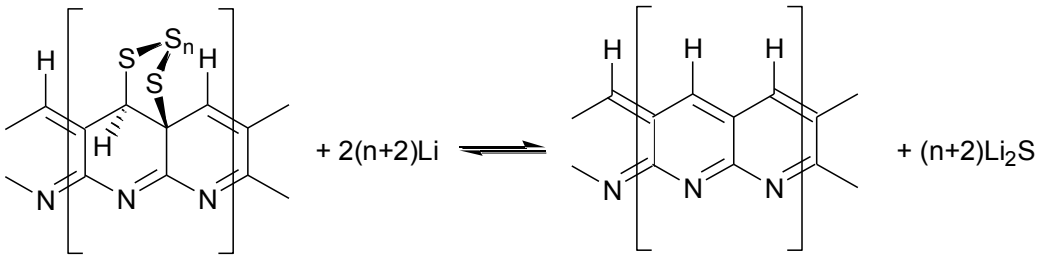

In discharging, the $–S_x–$ chain is first broken to form $–S_yLi$ and $–S_{x–y}Li$ segments, whose ends are covalently bonded to the polymer backbones. With the discharge progressing, the insoluble Li_2S is formed on the conducting carbon surface and the values of the y and $(x − y)$ in the SPAN are gradually decreased until 1, at which further discharging results in the breakdown of the C–S bonds and meanwhile forms carbon conjugated bonds. As indicated by Scheme 2, the final discharge products are a mixture of the conjugated polymer backbone and Li_2S. In the following charging, the conjugated polymer backbone first loses electrons to form delocalized radical cations, which immediately trap Li_2S to form C–SLi seeds, further charging results in the growth of the sulfur chain from the C–SLi seeds. When no Li_2S is available around the reaction sites, two grown C–SLi segments are electrochemically closed to form a ring, a similar structure as the original. In the entire discharging and charging process, the redox reaction of the SPAN takes place between the solid SPAN and the solid Li_2S. Therefore, the Li/SPAN cell is fundamentally different from the conventional Li/S cells, in which the sulfur reduction involves multiple phase transitions, including in sequence solid-to-liquid, liquid-to-liquid, liquid-to-solid, and solid-to-solid transitions [23].

2.2.2. Cycling Characteristics of Li/SPAN Cell

Typical cycling characteristics of the Li/SPAN cells are displayed in Figure 3. In the first discharge, the Li/SPAN cell suffers from significant voltage hysteresis (polarization) and produces large amount of irreversible capacity, as indicated by Figure 3a. The similar voltage hysteresis also has been frequently observed from the initial discharge of other conversion electrode materials [24]. We contribute such a voltage hysteresis to the poor electrical contact of the initial grain boundaries between the SPAN and conducting carbon particles. This judgment can be indirectly supported by the very erratic differential capacity-potential response, as indicated by Figure 3b. Due to the uneven and poor electrical contact of the initial grain boundaries, the dQ/dE–E chart in the first discharge is very erratic but becomes much more stable in the following charge and very smooth in the 5th cycle.

The large amount of irreversible capacity in the first discharge is mainly due to the irreversible reduction of the short (low delocalized) conjugated carbon bonds in the small SPAN fragments, rather than the catalytic (irreversible) reduction of the electrolyte solvents on the surfaces of conducting carbon or electrode material particles as occurred in the conversion electrode materials [24]. Ascribed to the difference in the synthesis conditions and PAN sources that have proven to greatly affect the size and distribution of the SPAN fragments, a wide range CE from 62% to 87% has been reported for the first cycle of the Li/SPAN cells [7,8]. As shown by Table 2, the initial CE and reversible capacities in the 2nd cycle of the SPANs vary greatly even if the SPANs have the same sulfur content. This is

attributed to the influence of the size and distribution of the SPAN fragments on the delocalization degree (and further reversibility) of the conjugated carbon bonds. In particular, the specific capacity of sulfur in a SPAN reaches 1930 mAh g^{-1} [8], exceeding the theoretical value (1675 mAh g^{-1}) of elemental sulfur, when the 1st CE is promoted to 86% by employing PAN precursor with high molecular weight and narrow molecular weight distribution [5]. In this case, parts of the capacities by the delocalized conjugated carbon bonds become reversible and contribute to the overall capacity.

Figure 3. Electrochemical characteristics of a Li/SPAN cell (37% S in SPAN) and a Li/carbon black (CB) cell, respectively. (**a**) voltage profile of Li/SPAN cell; (**b**) differential capacity-potential plot of Li/SPAN cell; (**c**) irreversible capacity of carbon black; and (**d**) cycling performance of Li/SPAN cell.

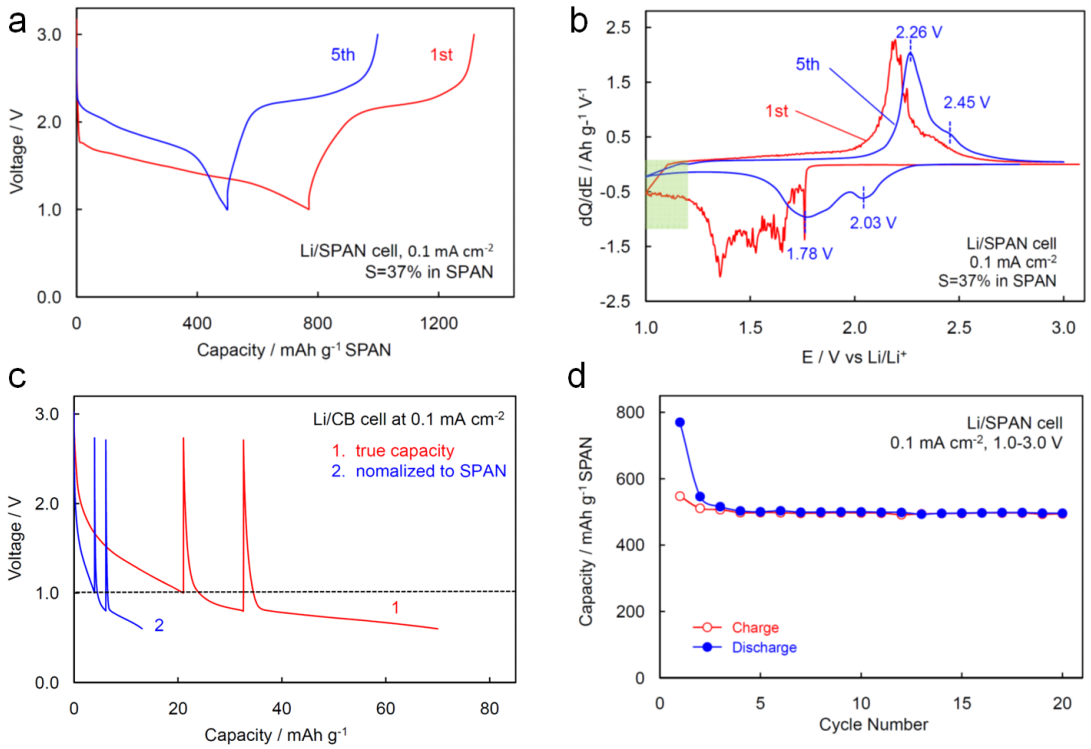

Table 2. Correlation of reversible capacity in 2nd cycle and initial coulombic efficiency (CE).

Synthesis Condition	S in SPAN wt%	CE %	Capacity at 2nd Cycle, mAh g^{-1}		Source
			vs. SPAN	*vs.* S	
350 °C, 5 h	42	81	726	1727	[7]
	42	86	811	1930	[8]
300 °C, 3 h, 4:1 S/PAN	48	75	477	993	[13]
	48	79	681	1419	–

In support of our judgment, we assembled and cycled a Li/carbon cell using the same carbon black (CB) and electrolyte solution, as shown by Figure 3c. From the open-circuit voltage to 1.0 V, the CB only produces a 21 mAh g^{-1} (*vs.* CB) of irreversible capacity, which equals to 3.9 mAh g^{-1} (*vs.* SPAN) if normalized by the weight percentage of SPAN in the electrode composition. Therefore, the contribution of the irreversible reduction of the electrolyte solvents to the initial irreversible capacity of the

Li/SPAN cell can be negligible. In addition, the dQ/dE–E chart shows that the irreversible reduction of the short conjugated carbon bonds mainly occurs in the voltage range from 1.2 to 1.0 V, as indicated by the shaded area in Figure 3b. This voltage range is slightly lower than those of the single carbon double bonds in the small organic solvents, such as vinylene carbonate (1.40 V *vs.* Li/Li^+) [25] and vinyl ethylene sulfite (1.48 V *vs.* Li/Li^+) [26].

Unlike the conventional Li/S batteries, the Li/SPAN cell only shows a slightly sloped voltage plateau in the discharging and charging voltage profile (see Figure 1a). This can be attributed to the solid-to-solid single-phase reaction of the SPAN as discussed in the electrochemical mechanism, and is in good agreement with those observed from the solid-state electrolyte Li/S batteries [27,28]. In the dQ/dE–E chart (Figure 3b), there are two pairs of distinct differential capacity peaks at 2.03/2.45 V and 1.78/2.26 V, respectively, which agrees with the previous report [4]. According to Structure–c, these two pairs of differential capacity peaks can be assigned to the redox reaction of the S–S bonds and S–C bonds, respectively. The excellent cyclability (770 mAh g^{-1} at 1st cycle and stabilized at 500 mAh g^{-1}) of the Li/SPAN cell, as shown in Figure 3d, can be again attributed to the solid-to-solid single-phase reaction of the SPAN, in which the dissolution of long-chain PS into organic electrolyte is entirely avoided. For the same reason, the fully charged Li/SPAN cell was reported to have no visible self-discharge over a month shelf storage [2], whereas the analogous Li/S cell suffered as high as 11% self-discharge after only one day of storage [29].

2.2.3. Chemical Compatibility of Electrolyte

It is well-known that the $LiPF_6$-carbonate based electrolytes currently used in the state-of-art Li-ion batteries are chemically incompatible with the Li/S batteries because of the strong nucleophilic reaction between the PS anion and carbonate solvents as well as the exchange reaction between the PS anion and fluorine in $LiPF_6$ [23,30,31]. It seems that the ether based electrolytes have been established as the standard for the conventional Li/S batteries [23]. However, Figure 4a shows that the Li/SPAN cell has much more stable capacity retention in the carbonate based electrolyte than in the ether based electrolyte. This can be attributed to two facts of: (1) entirely different reaction mechanism between the Li/SPAN and the conventional Li/S cells; and (2) significantly higher solubility of the long-chain PS in the ether based electrolytes than in the carbonate based electrolytes. As discussed in the electrochemical mechanism, the discharge and charge of the Li/SPAN cells undergo through a solid-to-solid single-phase reaction, in which all the SPAN, reduction intermediates (C–SLi), and final product (Li_2S) are insoluble in the organic solvents. The substantial insolubility greatly reduces the reactivity of sulfur species toward the carbonate solvents, which allows the use of carbonate based electrolytes in the Li/SPAN cells.

On the other hand, due to the high solubility of PS in the ether solvents, the ether based electrolyte promotes the rearrangement of $–S_x–$ chains in the SPAN to form soluble PS (a similar process as the disproportion). This phenomenon has been verified by the short voltage plateau at ~2.1 V in the first discharge of the Li/SPAN cell (Figure 4b). In the charging process, the ether based electrolyte promotes the Li_2S to be oxidized directly on the carbon surface to form PS and the resulting PS dissolves into the electrolyte. Therefore, the same problems as found in the conventional Li/S cells still exist in the Li/SPAN cell, resulting in fast capacity fading (Figure 4a). The above analyses suggest that the PS-insoluble carbonate based electrolytes are favorable for the Li/SPAN cells.

Figure 4. Effect of electrolyte solvents on the cycling performance of Li/SPAN cell (42% S in both SPANs). (**a**) capacity retention; and (**b**) voltage profile of the first cycle. Figure 4a was plotted from the data of [9] and Figure 4b is reproduced with permission of Elsevier from [7].

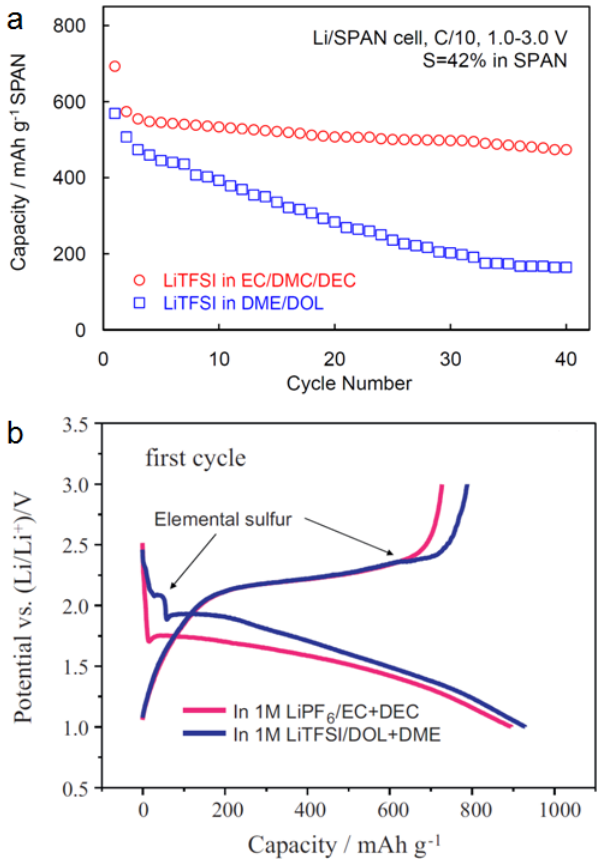

2.2.4. Over-Discharging and Over-Charging Characteristics

Asymmetric over-discharge and over-charge phenomena, as shown in Figure 5, have been reported for the Li/SPAN cells [4]. In particular, the Li/SPAN cell produced significant amounts of extra reversible capacities without causing visible degradation in the capacity and capacity retention when over-discharged to 0 V (see Figure 5a). However, the Li/SPAN cell did not produce any extra reversible capacities, and instead failed, when over-charged to above 3.8 V (see Figure 5b). These asymmetric phenomena can be reasonably explained by Scheme 2 and Structure–c. As suggested by Scheme 2, the carbons in the discharged SPAN are in conjugated state. In this case, the SPAN polymer backbones can act as the conducting polymer to provide extra capacities when over-discharged. The redox potential and reversibility of the organic solvents, conducting polymers and carbonaceous materials are varied with the delocalization degree of electrons, *i.e.*, the degree of carbon conjugation, for example, 1.4–1.5 V (irreversible) for single carbon double bonds [25,26], ~1.3 V (reversible) for linear n-doped polyacetylene [32], 1.0–1.2 V (irreversible) for the short conjugated carbon bonds in the SPAN as shown in Figure 3b, and 0.1–0.3 V (highly reversible) for plane graphite [33]. Therefore, it is reasonable to conclude that the extra capacities of the Li/SPAN cell below 1 V are due to the reversible redox of the highly delocalized conjugated carbon bonds in the desulfurized SPAN. On contrary, the conjugation carbon structure in the main backbone of the charged SPAN is repeatedly

broken by the C–S bonds (but still exists between C and N, as shown by Structure–c), which makes the SPAN electrochemically inactive. Therefore, no extra capacity can be released when the Li/SPAN cell is over-charged. The failure of the Li/SPAN cell at ~3.8 V is due to the anodic corrosion of the nickel current collector (foam) used in the SPAN cathode [4].

Figure 5. Over-discharging and over-charging characteristics of Li/SPAN cell (41.8% S in SPAN), in which the cathode active material was pressed onto a nickel foam and a current density of 0.25 mA cm^{-2} was used. (**a**) over-discharging to 0 V; and (**b**) over-charging toward 4 V. Reproduced with permission of Elsevier from [4].

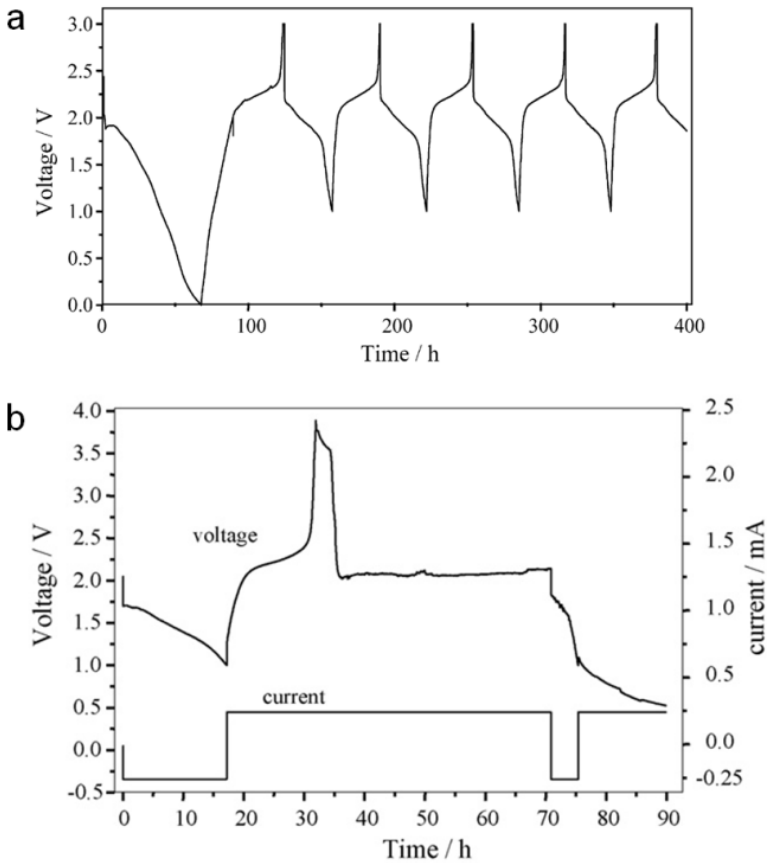

3. Experimental Section

As supplement for the previous literature, SPAN was synthesized by heating a 3:1 (wt) S/PAN mixture at 350 °C under nitrogen for 3 h. Resulting SPAN, having a sulfur content of 37 wt%, was coated onto a carbon-coated aluminum foil at a weight ratio of 80% SPAN, 15% carbon black (CB), and 5% poly(acrylonitrile-methyl methacrylate) (ANMMA, AN/MMA = 94:6, M_W = 100,000, Polysciences, Inc., Warrington, PA, USA) by using *N*-methyl pyrrolidinone solvent. On average, the cathode had a SPAN loading of 3.2–3.5 mg cm^{-2}. Using the same procedure and current collector, a carbon electrode consisting of 85 wt% CB and 15 wt% ANMMA was made. The electrode was punched into 1.27 cm^2 circular disks and dried at 100 °C under vacuum for 8 h prior to use. The electrolyte used was a 1.0 M $LiPF_6$ solution dissolved in a 3:7 (wt) mixture of ethylene carbonate (EC) and ethyl methyl carbonate (EMC) with water content less than 50 ppm. Using the above materials and a Celgard 3401 separator, the Li/SPAN and Li/CB coin cells, respectively, were assembled and cycled at

0.1 mA cm^{-2} between 1.0 and 3.0 V on a Maccor Series 4000 cycler (Maccor Inc., Tulsa, OK, USA). The specific capacity was referred as to the mass of SPAN, and those from previous publications were converted to the same specific capacity if not thus described.

4. Conclusions

Based on the analyses of this work, the chemical structure of the SPAN cathode materials can be generally described as the short $–S_x–$ chains covalently bonded to the cyclized, partially dehydrogenated, and ribbon-like PAN backbones. The significant voltage hysteresis and the large irreversible capacity in the first discharge are due to the poor electrical contact of the initial grain boundaries between the SPAN and conducting carbon particles and to the irreversible reduction of the short conjugated carbon bonds, respectively. The excellent cyclability of the Li/SPAN cells is attributed to the solid-to-solid single-phase redox reaction of the SPAN cathode materials, which entirely eliminates the redox shuttle of lithium polysulfide. The substantial insolubility of all the SPAN, reduction intermediates and final product in the carbonate based electrolytes greatly reduces the reactivity of sulfur species. Therefore, the Li/SPAN cells are chemically compatible with the $LiPF_6$–carbonate based electrolytes. The solid-to-solid single-phase reaction and the substantial insolubility of sulfur species in the carbonate solvents make the carbonate based electrolyte favorable for the Li/SPAN batteries. In addition, the highly delocalized conjugated carbon bonds can offer extra reversible capacities without causing visible performance degradation when the Li/SPAN cell is over-discharged.

Acknowledgments

The author is thankful to Cynthia A. Lundgren for her critical reading of the manuscript and valuable suggestions.

Conflicts of Interest

The author declares no conflict of interest.

References

1. Zhang, S.S. Sulfurized carbon: A class of cathode materials for high performance lithium/sulfur batteries. *Front. Energy Res.* **2013**, *1*, doi:10.3389/fenrg.2013.00010.
2. Wang, J.; Yang, J.; Xie, J.; Xu, N. A novel conductive polymer–sulfur composite cathode material for rechargeable lithium batteries. *Adv. Mater.* **2002**, *14*, 963–965.
3. Wang, J.; Yang, J.; Wan, C.; Du, K.; Xie, J.; Xu, N. Sulfur composite cathode materials for rechargeable lithium batteries. *Adv. Funct. Mater.* **2003**, *13*, 487–492.
4. He, X.; Pu, W.; Ren, J.; Wang, L.; Wang, J.; Jiang, C.; Wan, C. Charge/discharge characteristics of sulfur composite cathode materials in rechargeable lithium batteries. *Electrochim. Acta* **2007**, *52*, 7372–7376.
5. Pu, W.; He, X.; Wang, L.; Tian, Z.; Jiang, C.; Wan, C. Sulfur composite cathode materials: Comparative characterization of polyacrylonitrile precursor. *Ionics* **2007**, *13*, 273–276.

6. He, X.; Ren, J.; Wang, L.; Pu, W.; Wan, C.; Jiang, C. Electrochemical characteristics of sulfur composite cathode for reversible lithium storage. *Ionics* **2009**, *15*, 477–481.
7. Wang, L.; He, X.; Li, J.; Chen, M.; Gao, J.; Jiang, C. Charge/discharge characteristics of sulfurized polyacrylonitrile composite with different sulfur content in carbonate based electrolyte for lithium batteries. *Electrochim. Acta* **2012**, *72*, 114–119.
8. Wang, L.; He, X.; Li, J.; Gao, J.; Guo, J.; Jiang, C.; Wan, C. Analysis of the synthesis process of sulphur–poly(acrylonitrile)-based cathode materials for lithium batteries. *J. Mater. Chem.* **2012**, *22*, 22077–22081.
9. Fanous, J.; Wegner, M.; Grimminger, J.; Andresen, A.; Buchmeiser, M.R. Structure-related electrochemistry of sulfur–poly(acrylonitrile) composite cathode materials for rechargeable lithium batteries. *Chem. Mater.* **2011**, *23*, 5024–5028.
10. Fanous, J.; Wegner, M.; Grimminger, J.; Rolff, M.; Spera, M.B.M.; Tenzer, M.; Buchmeiser, M.R. Correlation of the electrochemistry of poly(acrylonitrile)–sulfur composite cathodes with their molecular structure. *J. Mater. Chem.* **2012**, *22*, 23240–23245.
11. Fanous, J.; Wegner, M.; Spera, M.B.M.; Buchmeiser, M.R. High energy density poly(acrylonitrile)–sulfur composite-based lithium–sulfur batteries. *J. Electrochem. Soc.* **2013**, *160*, A1169–A1170.
12. Doan, T.N.L.; Ghaznavi, M.; Zhao, Y.; Zhang, Y.; Konarov, A.; Sadhu, M.; Tangirala, R.; Chen, P. Binding mechanism of sulfur and dehydrogenated polyacrylonitrile in sulfur/polymer composite cathode. *J. Power Sources* **2013**, *241*, 61–69.
13. Konarov, A.; Gosselink, D.; Doan, T.N.L.; Zhang, Y.; Zhao, Y.; Chen, P. Simple, scalable, and economical preparation of sulfure–PAN composite cathodes for Li/S batteries. *J. Power Sources* **2014**, *259*, 183–187.
14. Jeddi, K.; Ghaznavi, M.; Chen, P. A novel polymer electrolyte to improve the cycle life of high performance lithium–sulfur batteries. *J. Mater. Chem. A* **2013**, *1*, 2769–2772.
15. Zhang, Y.; Zhao, Y.; Bakenov, Z.; Babaa, M.R.; Konarov, A.; Ding, C.; Chen, P. Effect of graphene on sulfur/polyacrylonitrile nanocomposite cathode in high performance lithium/sulfur batteries. *J. Electrochem. Soc.* **2013**, *160*, A1194–A1198.
16. Yu, X.; Xie, J.; Yang, J.; Huang, H.; Wang, K.; Wen, Z. Lithium storage in conductive sulfur-containing polymers. *J. Electroanal. Chem.* **2004**, *573*, 121–128.
17. Yu, X.; Xie, J.; Li, Y.; Huang, H.; Lai, C.; Wang, K. Stable-cycle and high-capacity conductive sulfur-containing cathode materials for rechargeable lithium batteries. *J. Power Sources* **2005**, *146*, 335–339.
18. Trevey, J.E.; Gilsdorf, J.R.; Stoldt, C.R.; Lee, S.H.; Liu, P. Electrochemical investigation of all-solid-state lithium batteries with a high capacity sulfur-based electrode. *J. Electrochem. Soc.* **2012**, *159*, A1019–A1022.
19. Wen, Z.; Lu, D. Fabrication and electrochemical performance of polyacrylonitrile-S/carbon composite as cathode for lithium ion batteries. *J. Electrochem. Soc.* **2013**, *160*, A2311–A2314.
20. Unemoto, A.; Gambe, Y.; Komatsu, D.; Honma, I. Development of high capacity all-solid-state lithium battery using quasi-solid-state electrolyte containing tetraglyme–Li-TFSA equimolar complexes. *Solid State Ionics* **2014**, *262*, 765–768.

21. Ferrari, A.C. Raman spectroscopy of graphene and graphite: Disorder, electron–phonon coupling, doping and nonadiabatic effects. *Solid State Commun.* **2007**, *143*, 47–57.
22. Bond Dissociation Energies in Simple Molecules. Available online: http://www.nist.gov/data/nsrds/NSRDS-NBS31.pdf (assessed on 17 July 2014).
23. Zhang, S.S. Liquid electrolyte lithium/sulfur battery: Fundamental chemistry, problems, and solutions. *J. Power Sources* **2013**, *231*, 153–162.
24. Ponrouch, A.; Taberna, P.; Simon, P.; Palacin, M.R. On the origin of the extra capacity at low potential in materials for Li batteries reacting through conversion reaction. *Electrochim. Acta* **2012**, *61*, 13–18.
25. Zhang, X.; Kostecki, R.; Richardson, T.J.; Pugh, J.K.; Ross, P.N. Electrochemical and infrared studies of the reduction of organic carbonates. *J. Electrochem. Soc.* **2001**, *148*, A1341–A1345.
26. Yao, W.; Zhang, Z.; Gao, J.; Li, J.; Xu, J.; Wang, Z.; Yang, Y. Vinyl ethylene sulfite as a new additive in propylene carbonate-based electrolyte for lithium ion batteries. *Energy Environ. Sci.* **2009**, *2*, 1102–1108.
27. Lin, Z.; Liu, Z.; Fu, W.; Dudney, N.J.; Liang, C. Lithium polysulfidophosphates: A family of lithium-conducting sulfur-rich compounds for lithium–sulfur batteries. *Angew. Chem. Int. Ed.* **2013**, *52*, 7460–7463.
28. Nagao, M.; Hayashi, A.; Tatsumisago, M. Electrochemical performance of all-solid-state Li/S batteries with sulfur-based composite electrodes prepared by mechanical milling at high temperature. *Energy Technol.* **2013**, *1*, 186–192.
29. Zhang, S.S.; Tran, D. How a gel polymer electrolyte affects performance oflithium/sulfur batteries. *Electrochim. Acta* **2013**, *114*, 296–302.
30. Gao, J.; Lowe, M.A.; Kiya, Y.; Abruna, H.D. Effects of liquid electrolytes on the charge–discharge performance of rechargeable lithium/sulfur batteries: Electrochemical and in-situ X-ray absorption spectroscopic studies. *J. Phys. Chem. C* **2011**, *115*, 25132–25137.
31. Yim, T.; Park, M.S.; Yu, J.S.; Kim, K.J.; Im, K.Y.; Kim, J.H.; Jeong, G.; Jo, Y.N.; Woo, S.; Kang, K.S.; *et al.* Effect of chemical reactivity of polysulfide toward carbonate-based electrolyte on the electrochemical performance of Li–S batteries. *Electrochim. Acta* **2013**, *107*, 454–460.
32. Shacklette, L.W.; Elsenbaumer, R.L.; Baughman, R.H. Electrochemical cells employing polyacetylene and poly(*p*-phenylene) as active materials. *J. Phys. Colloq.* **1983**, *44*, doi:10.1051/jphyscol:19833111.
33. Scrosati, B.; Garche, J. Lithium batteries: Status, prospects and future. *J. Power Sources* **2010**, *195*, 2419–2430.